

*Work supported in part by the National Science Foundation under Grant No. NSF GP 14521.

†E. I. DuPont Fellow, 1969–70.

¹T. P. Wangler *et al.*, Phys. Letters **9**, 71 (1964); R. Armenteros *et al.*, *ibid.* **9**, 207 (1964); D. H. Miller *et al.*, *ibid.* **15**, 74 (1965); S. P. Almeida *et al.*, *ibid.* **16**, 184 (1965); A. R. Erwin *et al.*, Nucl. Phys. **B9**, 364 (1966); J. Bartsch *et al.*, Phys. Letters **22**, 357 (1966); J. M. Bishop *et al.*, Phys. Rev. Letters **16**, 1069 (1966); B. C. Shen *et al.*, *ibid.* **17**, 726 (1966); W. de Baere *et al.*, Nuovo Cimento **49A**, 373 (1967); G. Bassompierre *et al.*, Phys. Letters **26B**, 30 (1967); J. C. Berlinghieri *et al.*, Phys. Rev. Letters **18**, 1087 (1967); D. J. Crennell *et al.*, *ibid.* **19**, 44 (1967); P. J. Dornan *et al.*, *ibid.* **19**, 271 (1967); G. Goldhaber *et al.*, *ibid.* **19**, 972 (1967); J. Bartsch *et al.*, Nucl. Phys. **B8**, 9 (1968); C. Y. Chien *et al.*, Phys. Letters **28B**, 143 (1968); F. Schweingruber *et al.*, Phys. Rev. **166**, 1317 (1968); J. C. Park *et al.*, *ibid.* **174**, 2165 (1968); J. C. Park *et al.*, Phys. Rev. Letters **20**, 171 (1968); D. Denegri *et al.*, *ibid.* **20**, 1194 (1968); F. Bomse *et al.*, *ibid.* **20**, 1519 (1968); J. M. Bishop *et al.*, Nucl. Phys. **B9**, 403 (1969); A. Astier *et al.*, *ibid.* **B10**, 65 (1969); G. Alexander *et al.*, *ibid.* **B13**, 503 (1969); D. C. Colley *et al.*, Nuovo Cimento **59A**, 519 (1969); B. Werner *et al.*, Phys. Rev. **188**, 2023 (1969); J. Andrews *et al.*, Phys. Rev. Letters **22**, 731

(1969); Hsieh Jen-Shu *et al.*, Nucl. Phys. **B18**, 17 (1970); M. S. Farber *et al.*, Phys. Rev. D **1**, 78 (1970).

²R. T. Deck, Phys. Rev. Letters **13**, 169 (1964).

³Although the Q enhancement is clearly present before any $N^*(1236)$ cuts are imposed on the data, we have chosen to show and to study the $K\pi\pi$ spectrum after eliminating those events in the N^* interval $1136 \text{ MeV}/c^2 \leq M(\pi^+\rho) \leq 1336 \text{ MeV}/c^2$. The $K^*(890)$ was defined as $840 \text{ MeV}/c^2 \leq M(K^+\pi^-) \leq 940 \text{ MeV}/c^2$. The ρ region was defined as $675 \text{ MeV}/c^2 \leq M(\pi^+\pi^-) \leq 825 \text{ MeV}/c^2$.

⁴In this study of the $K^*(890)$ decay the $K^+\pi^+\pi^-$ mass was required to be less than $1390 \text{ MeV}/c^2$ to reduce the contribution of the $K^*(1420)$ decay into $K^*(890)\pi$.

⁵E. L. Berger, Phys. Rev. **166**, 1525 (1968).

⁶It is easy to believe that an assignment based on meaningless criteria, e.g., the frame number, will produce identical distributions for the accepted and rejected hypotheses. The converse need not be true. For a given variable, such as the laboratory momentum, both the correct and incorrect hypotheses may produce identical distributions. It would be surprising if this were true for the distributions in all variables.

⁷There are 80 events in Group II for which both hypotheses have the $K^+\pi^-$ mass combination in the $K^*(890)$ mass region and 185 events without a $K^*(890)$ in either hypothesis.

PHYSICAL REVIEW D

VOLUME 3, NUMBER 11

JUNE 1971

π^-p Elastic Scattering in the c. m. Energy Range 1400–2000 MeV*

A. D. Brody, † R. J. Cashmore, A. Kernan, ‡ D. W. G. S. Leith, B. S. Levi, and B. C. Shen ‡
Stanford Linear Accelerator Center, Stanford University, Stanford, California 94305

and

J. P. Berge, § D. J. Herndon, R. Longacre, L. R. Price, || A. H. Rosenfeld, and P. Söding**
Lawrence Radiation Laboratory, University of California, Berkeley, California 94720

(Received 7 December 1970)

Total and differential cross sections for π^-p elastic scattering are presented at 35 energies between 1400 and 2000 MeV.

I. INTRODUCTION

In recent years a large amount of data has been accumulated on the elastic and charge-exchange channels of πN scattering. Several extensive phase-shift analyses¹⁻⁷ performed on these data have uncovered much of the complicated resonance structure up to energies of 2000 MeV. The data and phase-shift results have been summarized by a number of authors.⁸⁻¹¹ Resonance parameters from some of the recent analyses are listed in Table I.¹² Despite good qualitative agreements, quantitative discrepancies still exist among the various solutions. These discrepancies exist in part because of the multidimensional parameter

space explored and the different methods used, because of fluctuations between different experimental measurements, and finally, because the elastic data used are fairly insensitive to partial waves of low elasticity. Thus, the motivation for the present experiment was to fill the need for direct measurement of the inelastic channels. The systematic and rather complete set of measurements of the elastic channels, described in this paper, came as a by-product of this inelastic study.

We present below the first part of the results of a study of elastic and inelastic π^-p scattering at 35 momenta between 550 and 1600 MeV/c. Figure 1 illustrates the scope of the experiment. At each

TABLE I. $S=0$ baryon resonances.

Phase-shift ^a analysis	$I = \frac{1}{2}$ states											
	M	Γ	x	M	Γ	x	M	Γ	x	M	Γ	x
	P_{11} (1470)			D_{13} (1520)			S_{11} (1535)			D_{13} (1700)		
1	1470	255	0.68	1510	125	0.54	1535	155	...			
2	1505	205	0.68	1515	110	0.54	1515	105	...		Possible	
3	Definite			1526 ^b	114 ^b	0.57 ^b	1548 ^b	116 ^b	0.326 ^b		Possible	
4	1466	211	0.658	1541	149	0.509	1591	(268) ^c	0.696
5	1470	211	0.66	1520	114	0.57	1550	116	0.33	1730		
6	1466	211	0.66	1526	115	0.57	1540	160	0.3	1680		
7	1462	391	0.49	1512	106	0.45	1502	(36)	0.36		Not present	
8	1436	224	0.46	1512	125	0.49	1499	53	0.35		Not present	
Average	1468	244	0.61	1520	120	0.53	1535	118	0.39	1705		
±	±19	±62	±0.09	±10	±13	±0.04	±28	±35	±0.14	±25		
	D_{15} (1670)			F_{15} (1688)			S_{11} (1700)			P_{11} (1780)		
1	1680	135	0.41	1690	110	0.64	1710	260	...		Probable	
2	1655	105	0.41	1680	105	0.64	1665	110	...		Probable	
3	Definite			1692 ^b	132 ^b	0.68 ^b	1709 ^b	300 ^b	0.786 ^b		Probable	
4	1678	173	0.391	1687	177	0.56	1751	327	0.32
5	1680	173	0.391	1690	132	0.68	1710	300	0.79	1750	327	0.32
6	1678	175	0.391	1692	130	0.68	1709	300	0.79	1860	270	0.32
7	1669	115	0.50	1685	104	0.54	1766	404	0.56	1770	445	0.43
8	1667	115	0.43	1684	123	0.54	1671	121	0.51	(1867)	(525)	0.30
9												
Average	1672	142	0.42	1688	127	0.62	1706	256	0.69	1783	350	0.34
±	±10	±29	±0.04	±4	±22	±0.06	±31	±98	±0.13	±45	±63	±0.05
	P_{13} (1860)			F_{17} (1990)			D_{13} (2040)			G_{17} (2190)		
1	Ambiguous ^d			d			d			d		
2	Ambiguous ^d			d			d			d		
3	Ambiguous ^d			d			d			d		
4	1863	296	0.207	1983	225	0.128	2057	293	0.26	2265	298	0.349
5	1860	296	0.21	2030	290	0.11	2190	300	0.35
6	1900	325	0.25	1995	250	0.09	2040	240	0.15	2265	300	0.35
7	1844	449	0.40	e			d			(1906) ^e	(319) ^e	(0.14) ^e
8	1854	307	0.26	e			d			e		
9	1860	2000	2030	2000		
Average	1864	335	0.27	1989	238	0.109	2039	274	0.17	2180	299	0.350
±	±17	±58	±0.07	±6	±12	±0.019	±11	±24	±0.06	±35	±2	±0.001

momentum the following reactions were measured:

$$\pi^- p \rightarrow \pi^- p \quad (1)$$

$$\rightarrow n\pi^+\pi^- \quad (2)$$

$$\rightarrow p\pi^-\pi^0 \quad (3)$$

$$\rightarrow \Lambda^0 K^0 \quad (4)$$

$$\rightarrow \Sigma^0 K^0, \Sigma^- K^+ \quad (5)$$

This paper concerns only reaction (1). Reactions (2) and (3) are currently being studied both in terms of a quasi-two-body final state and in terms of a three-body analysis. The results of these studies as well as the strange-particle data will be

presented in separate communications. Finally, we are extending the experiment to higher momenta, up to 2.25 BeV/c, as illustrated by the dashed lines in Fig. 1.

II. EXPERIMENTAL DETAILS AND FILM MEASUREMENT

A. Experimental Details

The experiment was performed using the 30-in. MURA hydrogen bubble chamber (HBC) at the Argonne National Laboratory and the 72-in. Alvarez HBC at Berkeley. The Argonne exposure consists of ~500 000 pictures taken at 26 momenta between 550 and 865 MeV/c and between 1060 and

TABLE I (Continued)

Phase-shift ^a analysis	$I = \frac{3}{2}$ states											
	M	Γ	x	M	Γ	x	M	Γ	x	M	Γ	x
	S_{31} (1650)			P_{33} (1690)			D_{33} (1670)			F_{35} (1890)		
1	1695	250	...	Ambiguous			Possible			Possible		
2	1650	130	...	Ambiguous			Possible			Possible		
3	Definite			Possible			Ambiguous			Probable		
4	1635	177	0.284	1688	281	0.098	1691	269	0.14	1913	350	0.16
5	1640	177	0.28	1690	281	0.1	1690	269	0.14	1910	350	0.16
6	1635	180	0.28	1690	240	0.08	1690	300	0.13	1910	380	0.15
7	1617	141	0.28	Not present			1649	188	0.12	1841	136	0.2
8	1623	140	0.25	Not present			1650	174	0.13	1852	150	0.19
Average	1643	151	0.27	1689	267	0.093	1674	240	0.13	1885	273	0.17
\pm	± 24	± 89	± 0.12	± 2	± 19	± 0.009	± 20	± 50	± 0.01	± 32	± 107	± 0.02
	P_{31} (1910)			D_{35} (1960)			F_{37} (1950)			P_{33} (2160)		
1	Ambiguous ^d			Ambiguous ^d			1975	180	0.57	d		
2	Ambiguous ^d			Ambiguous ^d			1980	140	...	d		
3	Probable ^d			d			Definite			Possible ^d		
4	1934	339	0.30	1954	311	0.154	1946	221	0.386			
5	1930	339	0.3	1950	221	0.39			
6	1930	425	0.25	1970	400	0.12	1946	220	0.39	2160	260	0.25
7	1914	290	0.18	d			1935	196	0.51	d		
8	1843	231	0.24	d			1935	212	0.39	d		
9				1950						
Average	1910	325	0.25	1958	356	0.14	1952	199	0.44	2160	260	0.25
\pm	± 38	± 64	± 0.04	± 9	± 44	± 0.02	± 19	± 28	± 0.07

^aSee Ref. 12 for various phase-shift analyses.

^bValues quoted by C. Lovelace, rapporteur talk at International Conference on Elementary Particles, Heidelberg, Germany, 1967, Ref. 7.

^cValues in parentheses have not been used in the averages.

^dThis state is very close to, or beyond, their highest energy.

^eGlasgow A has a G_{17} state at this mass, and Glasgow B may have an F_{17} and a G_{17} ; however, this energy is very close to their highest energy.

1600 MeV/c. The Berkeley exposure comprises about 200 000 pictures taken at 9 momenta between 925 and 1175 MeV/c. This latter film had been taken ten years previously, to study strange-particle events about the Λ, Σ threshold,¹³ but had not been used to investigate the two-prong events.

The Argonne film was taken during three separate exposures in 1967. The beam was the "7°" separated beam¹⁴ of the Zero Gradient Synchrotron (ZGS). The higher-momentum exposures used the mode shown in Figs. 2(a) and 2(b). Here, the first stage provided at slit 1 both a momentum focus in the horizontal plane and an image of the target in the vertical plane. The second stage provided a momentum focus at the final slit together with an image of the target in both planes. A simplified version of the beam, Fig. 2(c), was used for the low-momentum exposures (i.e., $p\pi < 1$ GeV/c). The low-energy pion flux was found to be much less than expected, and as a result it was not pos-

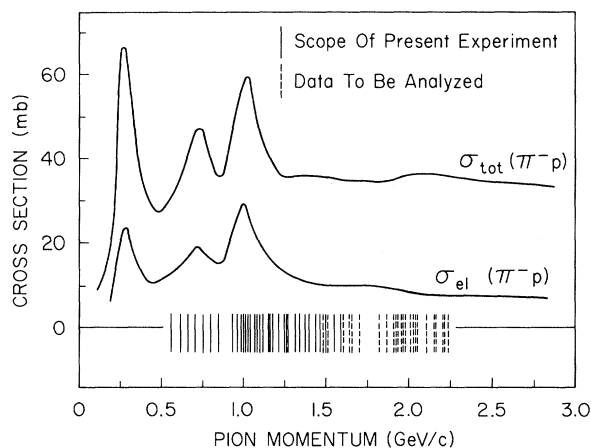


FIG. 1. Scope of the present experiment. The solid lines mark energies where the data have been analyzed. The dashed lines mark energies to which the experiment will be extended.

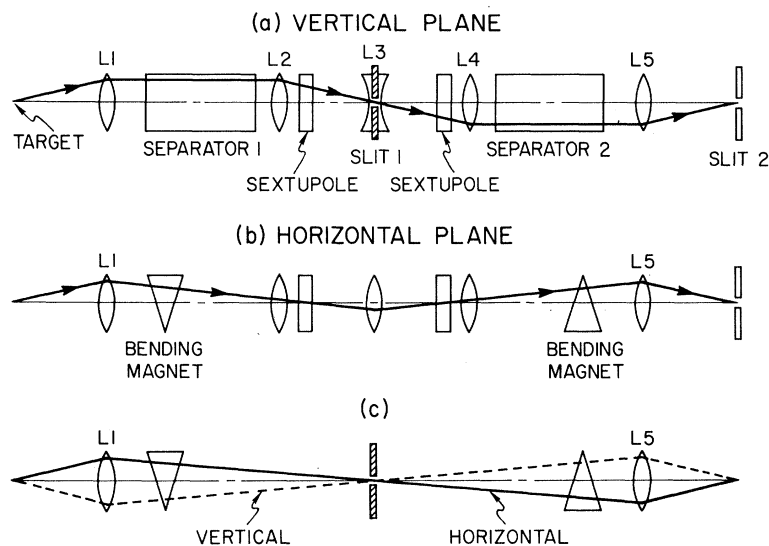


FIG. 2. Argonne beam optics. (a) and (b): Vertical and horizontal planes of the optics used for the second and third exposures. (c): Simplified mode used for the first exposure.

sible to obtain a useful beam below 580 MeV/c.

To produce an ideal shape (5 in. wide and 6 in. high) for the beam trajectory in the chamber, further quadrupoles were used after the final slit. Since the image at the final slit had little vertical divergence, it was most effective to rotate the first quadrupole 45° to couple optically the vertical and horizontal planes. The second quadrupole then increased the vertical divergence and decreased the horizontal divergence.

The high field of the 30-in. HBC and the low momentum of the beam made it necessary to raise the center of the chamber 7 in. above the center beam line, and then to pitch the beam downwards into the fringe field of the bubble-chamber magnet to obtain a good trajectory of the beam through the chamber. Finally, for momenta below 870 MeV/c it was further necessary to lower the HBC-magnet current from 20 000 A to 12 000 A, to maintain this trajectory.

The proton beam of the ZGS gave a pulse of pions once every 2.9 sec. For part of the exposure, the bubble chamber was triple-pulsed during each beam spill, allowing a rate of nearly 1 picture per second.

The π^- beam used for the Berkeley exposure is

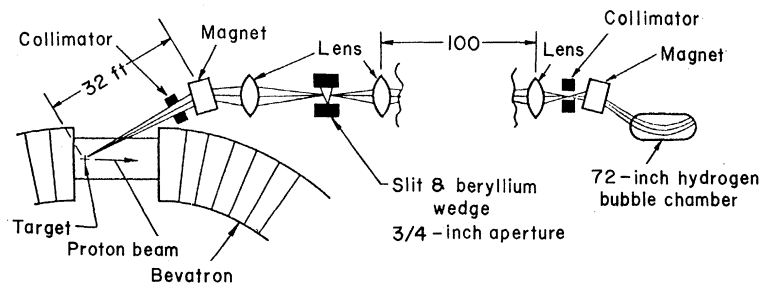


FIG. 3. Berkeley beam.

sketched in Fig. 3. It has been previously described¹⁵ for a momentum setting of 1030 MeV/c. The characteristics remain the same at the momenta used in the present experiment. In particular, the beam is characterized by good momentum resolution, the fractional momentum bite $\Delta p/p$ being on the order of $\pm 0.5\%$.

All beam interactions within the volume 34 cm wide, 122 cm long, and 9 cm deep were accepted from the 72-in. chamber, while for the 30-in. chamber, the fiducial volume was defined as 58 cm long, 58 cm wide, and 16 cm deep.

The coordinate system for both chambers is defined with the camera axis as the z axis and the beam coincident with the y axis: In the Alvarez chamber, the camera axis is tilted $7\frac{1}{2}^\circ$ with respect to the vertical axis.

The magnetic fields of both chambers were determined by extrapolating from previously measured field maps. These existed for the 72-in. chamber at magnet-current settings of 2400 A, 3500 A, and 4600 A. The measured values of the B_z at these currents were fitted with a 27-term polynomial expansion¹⁶ and the horizontal components were calculated to satisfy Maxwell's equations to third power in xy . These coefficients

TABLE II. Magnet currents and central field values.

Chamber	I (A)	Field (kG)	Momentum range (MeV/c)
72 in.	2400	10.254	956-995
	2600	11.025	1004-1024
	3102	13.85	924
	3690	14.54	1024-1042
	4600	17.77	1125-1174
30 in.	12 000	20.98	556-853
	20 000	32.566	853-1602

were scaled where necessary to the settings of 3102 A, 3690 A, 2600 A, and 4600 A used in the present experiment. The value of B_z at the center of the chamber was determined by looking at K^0 decays ($K^0 \rightarrow \pi^+ + \pi^-$) and elastic scatters. We required that the distribution in the unfit invariant mass of the π^+ and π^- agree with the accepted K^0 mass. We also required that the distributions in measured and fitted values of the momenta of each track in the 4C (elastic scatter) events agree. We found that both of these criteria were simultaneously satisfied in most regions of our film rather

easily.

The same procedure was adopted to determine the field of the 30-in. chamber. It was necessary to scale from the field map measured at 20 000 A down to 12 000 A. Two precautions were taken here. The field measurement at 20 000 A agreed with the design calculations to within 1%. Furthermore, the field shape was predicted to remain the same at lower current settings. As an additional check, the film taken at 853 MeV/c was divided between the two values of the field. The elastic scatters from the two fields were compared and no discernible differences were detected.

Table II summarizes the currents and central values of the fields used.

The optical constants required by the fitting programs were determined by making a 12-parameter least-squares fit of measured fiducials to their known positions, using the program WEASEL. For the 72-in. HBC, 13 fiducials were measured, with many sets of measurements being obtained throughout the entire exposure. Several sets of measurements were averaged, whenever appropriate, with the program MONKEY. Each set of constants was checked by comparing measured quantities with

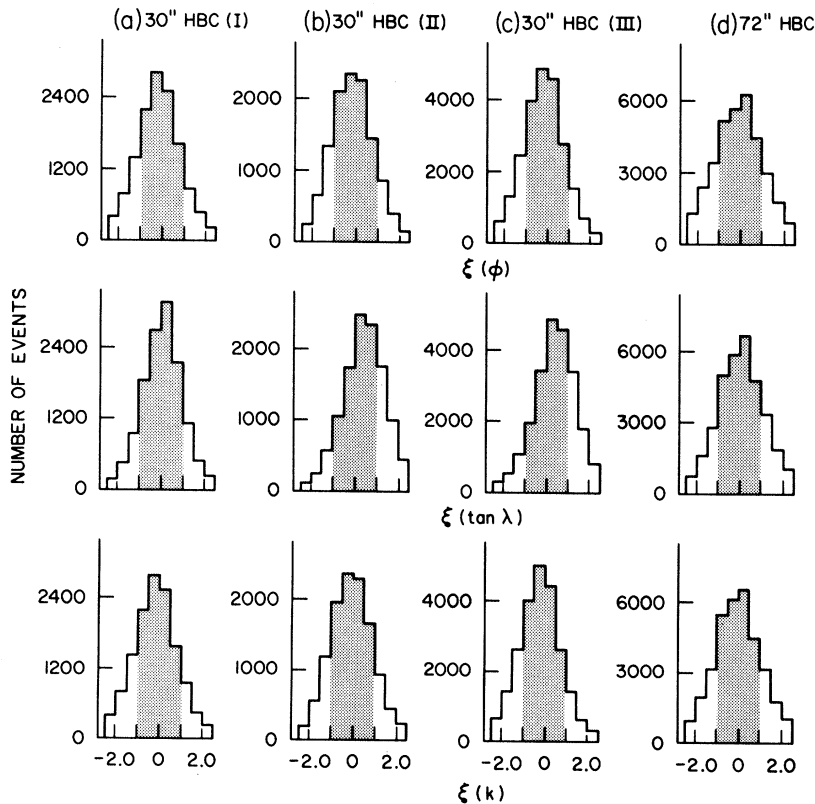


FIG. 4. Beam-track pull quantities for each exposure (a)–(c): 30-in. HBC. (d): 72-in. HBC.

$$\xi(X) = \frac{(X_{\text{meas}} - X_{\text{fit}})}{\langle X_{\text{meas}} - X_{\text{fit}} \rangle}$$

corresponding fitted quantities of 4C elastic-scattering events in all parts of the chamber. Although there was poor agreement at the edges of the chamber, satisfactory results were obtained within the fiducial volume. The pull distributions in Fig. 4(d) reflect the quality of spatial reconstruction.

The same procedure was used to determine the optical constants for the 30-in. MURA HBC. However, the reconstruction was slightly less satisfactory, because there were not enough visible fiducials to enable determination of the high-order distortion parameters. The pull distributions are given in Figs. 4(a)–4(c).

B. Measurement

The bubble-chamber film was scanned at SLAC and an LRL Spiral Reader was used to measure the events. The scanners at SLAC recorded all two-prong events. Events in which the beam track disappeared for more than a projected length of 3 mm before the vertex were classified as 0-prong, 1-vee events. Events were rejected if obscured in any way or if the beam track was less than 3 cm long. No bias is introduced by these rejects. Events in which both outgoing tracks were less than 1 cm were also rejected, introducing a loss of reactions with short protons. Such events correspond to c.m. scattering angles which are not included in our results and analysis (see Sec. IV). However, a further bias is expected due to loss of short, dipping protons, and correction for this bias will be discussed in Sec. III.

The scanning efficiency was evaluated by rescanning

approximately 20% of the Argonne film and 10% of the Berkeley film. The master lists from the first and second scans were then compared by the computer program CONFLICT, which lists all discrepancies. These discrepancies were examined again on the scan table to determine whether they were valid events. Following this procedure, the combined scan efficiency was found to be 97%.

The film was measured on an LRL Spiral Reader,¹⁷ a semiautomatic film digitizing machine. The reader digitizations are connected into tracks by a FORTRAN filter program POOH,¹⁸ With this program it is difficult to fit steeply dipping tracks, and the loss of such tracks constituted a bias which will be examined in the next section.

III. DATA ANALYSIS

The measured two-prong events are processed by the SIOUX-ARROW system programs. SIOUX consists of a three-view geometry program for spatial reconstruction and a fitting program which tries, in this experiment, each of the following hypotheses:

$$\pi^- p \rightarrow \pi^- p \quad (1)$$

$$\rightarrow n \pi^+ \pi^- \quad (2)$$

$$\rightarrow p \pi^- \pi^0. \quad (3)$$

Since the 4C elastic hypothesis is more highly constrained than the 1C inelastic hypotheses, there is little contamination of these elastic events. Contamination is further reduced by the requirement that the ionization measured by the Spiral Reader be consistent with the fitted track momen-

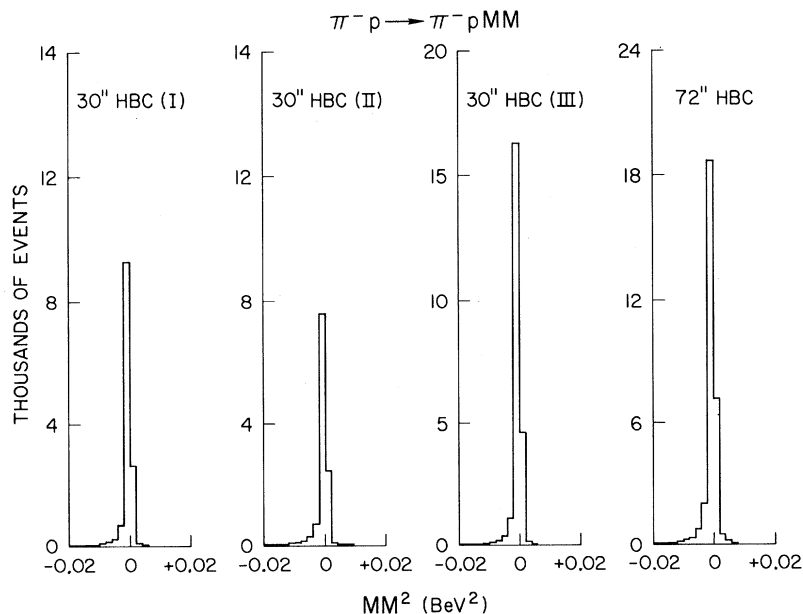


FIG. 5. Missing mass squared in the reaction $\pi^- p \rightarrow \pi^- p$ MM for the 4C elastic events. The shift toward the negative side is expected in such missing-mass plots (Ref. 19).

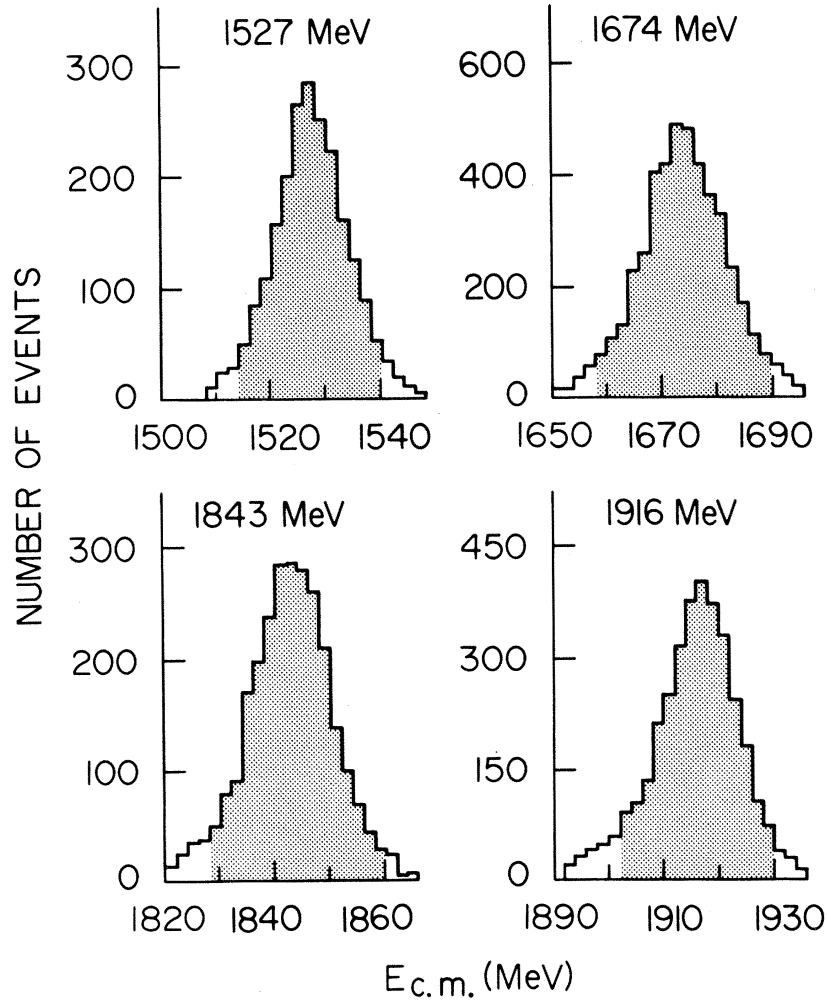


FIG. 6. Center-of-mass energies from 4C events for typical roll regions of the film. Shading indicates the data used in the analysis.

tum. The clean separation of the final-sample 4C events is illustrated in Fig. 5, where we plot the square of the missing mass in the reaction

$$\pi^-p \rightarrow \pi^-pMM.$$

This histogram is sharply peaked at zero, with a slight pull to the negative side, as expected in plots of this type.¹⁹

The center-of-mass energies are determined for each region of film from the fitted distributions of the 4C elastic events. Sample distributions are shown in Fig. 6. The beam has a low-energy tail. In determining the mean value of the c.m. energy, cutoffs were applied to the data. These cutoffs are given in Table V, below.

Because of the high momentum resolution of the Berkeley beam, the technique of "beam averaging" was used in processing this film. The momentum for a given event was a weighted average of "beam

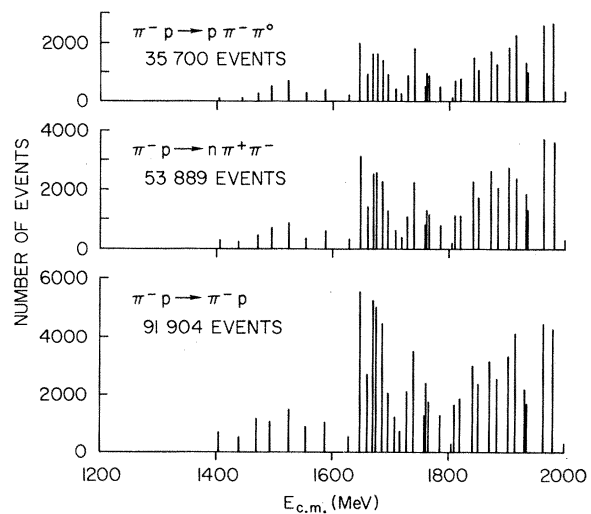


FIG. 7. Number of events of the three reaction types processed at each energy.

average" and measured momenta, calculated from the expression

$$\bar{p} = \frac{p_{\text{meas}}/(\Delta p_{\text{meas}})^2 + p_{\text{B.A.}}/(\Delta p_{\text{B.A.}})^2}{1/(\Delta p_{\text{meas}})^2 + 1/(\Delta p_{\text{B.A.}})^2}.$$

In order to determine the beam average momentum and its associated error, the following procedure was used. All events were processed through SIOUX without beam averaging. Those events fitting the 4C elastic-scattering hypothesis with a $\chi^2 \leq 10$ were used to determine the average value of the beam momentum, $p_{\text{B.A.}}$, and its error, $\Delta p_{\text{B.A.}}$.

The efficiency for passing events through the measuring process and the filtering program was

found to be 97% after the first measurement of the 72-in. HBC film. We made a repeat measurement of about 17000 events and found the combined efficiency then to be 99%. All of the 30-in. HBC film was measured twice except for 43% which had unambiguous fits on the first measurement. The combined efficiency after the second measurement for all events in the 30-in. chamber was 93%. Those events which failed twice were examined on the scan table, and no evidence for topological bias was found apart from the bias against short protons mentioned previously. The number of events of each reaction type (1), (2), or (3) which were processed is given in Fig. 7 and in Table III. Figure 8 shows the χ^2 distributions from our

TABLE III. Events processed at each energy.

Exposure	$E_{\text{c.m.}}$ (MeV)	$p_{\text{lab}}^{\pi^-}$ (MeV/c)	4C events $\chi^2 \leq 14$	1C $n\pi\pi$ events $\chi^2 \leq 8$	1C $p\pi\pi$ events $\chi^2 \leq 8$	
30-in. HBC (I)	1406	556	648	255	80	
	1440	609	500	215	82	
	1472	660	1110	418	245	
	1496	699	1854	675	499	
	1527	750	2337	832	701	
	1556	797	826	340	272	
	1589	853	997	579	387	
	1709	1067	1141	585	400	
	1730	1105	1954	1046	836	
	1762	1165	2230	1231	899	
30-in. HBC (II)	1811	1259	1544	1096	651	
	1843	1322	2777	2172	1337	
	1872	1381	2920	2443	1568	
	1904	1444	3160	2616	1694	
	1935	1509	1606	1288	886	
30-in. HBC (III)	1720	1084	687	392	262	
	1761	1161	1200	786	488	
	1787	1212	1210	798	476	
	1806	1250	292	188	122	
	1821	1278	1740	1098	687	
	1853	1340	2213	1649	979	
	1885	1404	2392	1970	1180	
	1916	1469	3792	3203	2105	
	1933	1503	1972	1735	1177	
	1963	1567	4113	3512	2405	
	1980	1602	3957	3416	2458	
	72-in. HBC	1628	924	537	358	200
		1647	956	5482	3169	1968
1660		979	2697	1430	879	
1669		995	5127	2562	1603	
1674		1004	4966	2673	1568	
1685		1024	4398	2281	1409	
1695		1042	2206	1299	871	
1740		1125	3594	2259	1786	
1766		1174	1733	1120	854	
Totals				79 911	51 477	33 880

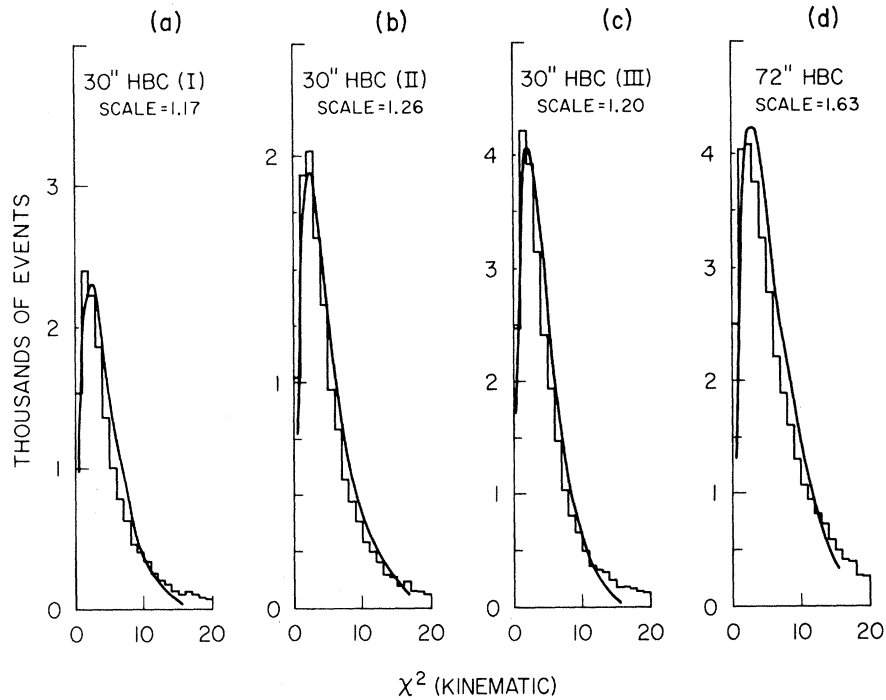


FIG. 8. χ^2 distributions for each exposure. (a)–(c): 30-in. HBC. (d): 72-in. HBC. Smooth curves are the scaled theoretical distributions normalized to the total number of events.

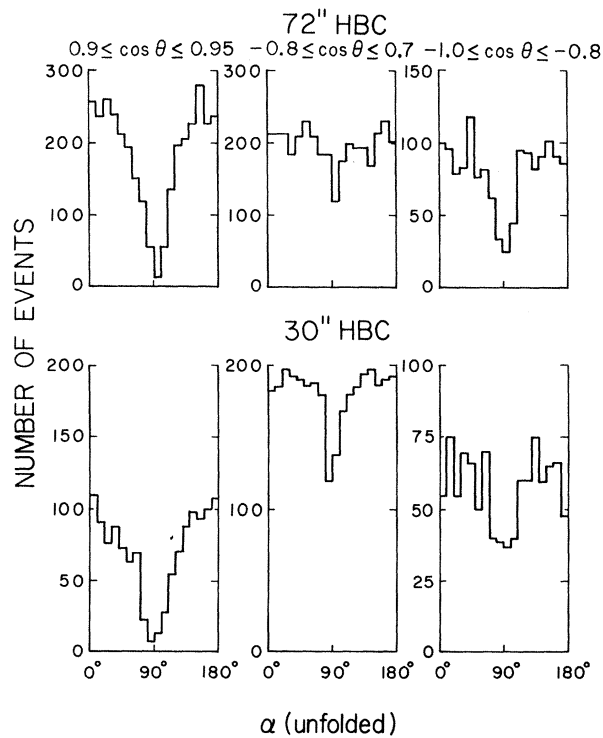


FIG. 9. Azimuthal angle for forward, middle, and backward regions of pion-production angle. α is defined as the angle between the normal to the scattering plane and the camera axis.

TABLE IV. Azimuthal correction factors and errors.

$E_{c.m.}$ (MeV)	0.9 to 0.95	0.8 to 0.9	0.7 to 0.8	-0.8 to 0.7	-1.0 to -0.8
1406	1.50±0.20	1.25±0.10	1.10±0.08	1.08±0.04	1.02±0.08
1440	1.50±0.20	1.25±0.10	1.10±0.08	1.08±0.04	1.02±0.08
1472	1.50±0.20	1.25±0.10	1.10±0.08	1.08±0.04	1.02±0.08
1496	1.45±0.18	1.20±0.08	1.02±0.07	1.05±0.04	1.02±0.10
1527	1.45±0.14	1.13±0.07	1.10±0.07	1.01±0.03	1.10±0.10
1556	1.60±0.22	1.25±0.10	1.12±0.10	1.06±0.04	1.10±0.13
1589	1.60±0.22	1.25±0.10	1.12±0.10	1.06±0.04	1.10±0.13
1628	1.30±0.20	1.08±0.12	1.12±0.20	1.0±0.07	1.18±0.18
1647	1.28±0.06	1.08±0.04	1.05±0.05	1.05±0.03	1.14±0.06
1660	1.14±0.07	1.02±0.05	1.01±0.07	1.05±0.04	1.17±0.08
1669	1.22±0.05	1.07±0.04	1.04±0.05	1.04±0.03	1.16±0.07
1674	1.17±0.05	1.08±0.04	1.00±0.05	1.11±0.03	1.15±0.07
1685	1.29±0.07	1.07±0.05	1.07±0.06	1.05±0.04	1.12±0.06
1695	1.25±0.08	1.13±0.06	1.07±0.08	1.02±0.04	1.04±0.08
1709	1.30±0.10	1.08±0.05	1.05±0.06	1.03±0.04	1.10±0.09
1720	1.22±0.10	1.04±0.07	1.02±0.08	1.10±0.07	1.00±0.11
1730	1.30±0.10	1.08±0.05	1.05±0.06	1.03±0.04	1.10±0.09
1740	1.24±0.06	1.10±0.04	1.05±0.05	1.07±0.03	1.20±0.09
1761	1.22±0.10	1.04±0.07	1.02±0.08	1.10±0.07	1.00±0.11
1762	1.19±0.07	1.13±0.07	1.03±0.06	1.07±0.04	1.17±0.10
1766	1.18±0.08	1.06±0.06	1.04±0.07	1.01±0.05	1.20±0.15
1787	1.11±0.07	1.08±0.05	1.05±0.06	1.05±0.04	1.01±0.10
1806	1.11±0.07	1.08±0.05	1.05±0.06	1.05±0.04	1.01±0.10
1811	1.18±0.11	1.05±0.07	1.09±0.09	1.00±0.05	1.00±0.11
1821	1.11±0.07	1.08±0.05	1.05±0.06	1.05±0.04	1.01±0.10
1843	1.17±0.06	1.07±0.05	1.10±0.08	1.06±0.05	1.07±0.11
1853	1.10±0.07	1.02±0.05	1.07±0.08	1.06±0.05	1.04±0.13
1872	1.10±0.06	1.05±0.04	1.10±0.07	1.03±0.04	1.05±0.10
1885	1.12±0.07	1.05±0.06	1.04±0.08	1.06±0.06	1.10±0.14
1904	1.05±0.05	1.06±0.04	1.09±0.07	1.04±0.04	1.11±0.14
1916	1.25±0.06	1.08±0.05	1.15±0.08	1.11±0.05	1.00±0.11
1933	1.16±0.08	1.13±0.06	1.16±0.10	1.10±0.06	1.12±0.20
1935	1.08±0.08	1.00±0.06	1.08±0.09	1.10±0.07	1.15±0.25
1963	1.12±0.05	1.07±0.05	1.01±0.01	1.05±0.04	1.15±0.15
1980	1.22±0.06	1.20±0.07	1.10±0.08	1.09±0.04	1.05±0.15

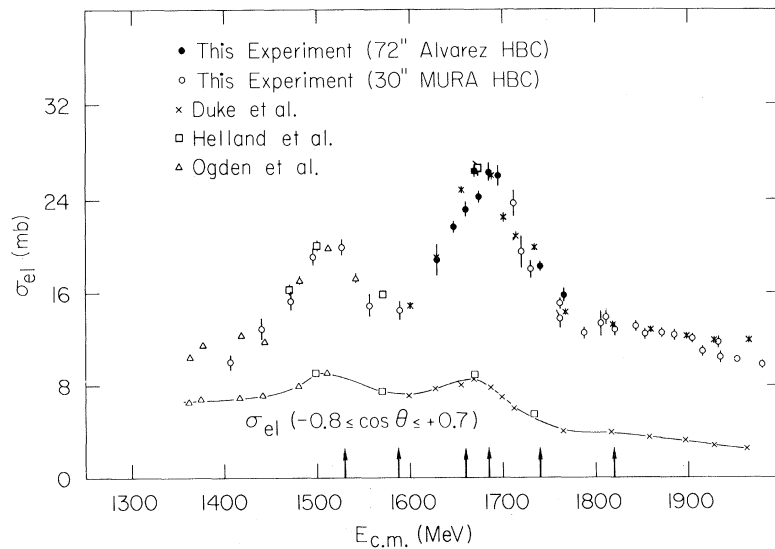


FIG. 10. π^-p elastic-cross-section measurements of Duke *et al.* (Ref. 20), Helland *et al.* (Ref. 21), Ogden *et al.* (Ref. 22), and this experiment. The lower curve is the cross section integrated over the region used for normalization, $-0.8 \leq \cos\theta \leq +0.7$. The arrows indicate energies chosen for comparison of differential cross sections with the results of phase-shift analyses.

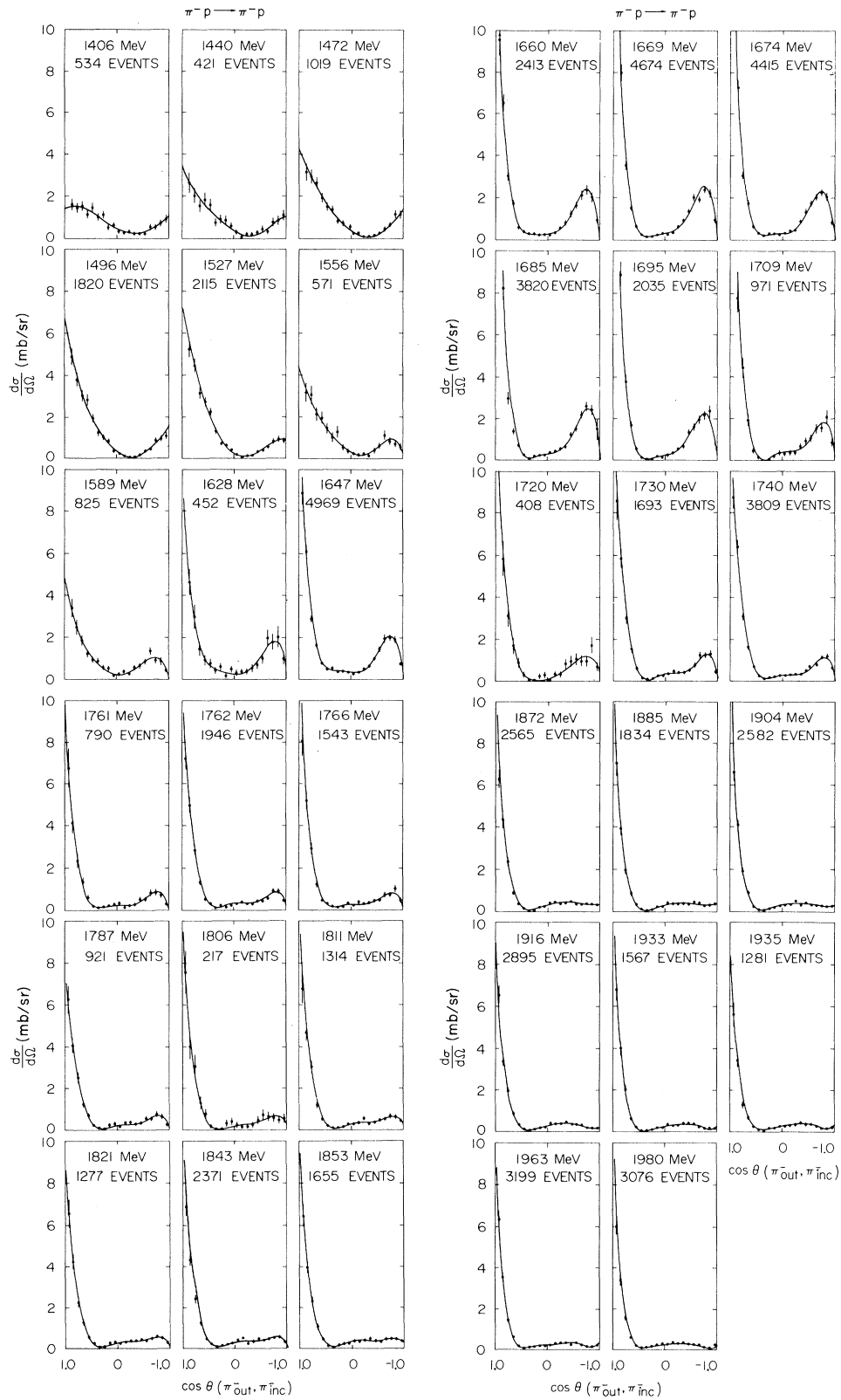


FIG. 11. π^-p differential cross sections measured in this experiment. The smooth curves represent the best fit by an expansion in Legendre polynomials.

TABLE V. Legendre polynomial coefficients. $d\sigma/d\Omega = \sum_n A_n P_n(\cos\theta)$.

$E_{c.m.}$ (MeV)	1406	1440	1472	1496	1527	1556	1589
Low-energy cutoff	1394	1428	1456	1482	1514	1544	1576
High-energy cutoff	1418	1452	1486	1510	1540	1568	1602
A_0	0.82 ± 0.05	1.02 ± 0.08	1.22 ± 0.06	1.52 ± 0.06	1.58 ± 0.06	1.19 ± 0.08	1.15 ± 0.07
A_1	0.61 ± 0.12	1.09 ± 0.19	1.48 ± 0.16	2.23 ± 0.15	2.45 ± 0.15	1.45 ± 0.19	1.22 ± 0.17
A_2	0.54 ± 0.17	1.31 ± 0.27	1.66 ± 0.22	2.42 ± 0.21	2.61 ± 0.20	1.52 ± 0.27	1.69 ± 0.24
A_3	-0.46 ± 0.21	-0.04 ± 0.31	-0.08 ± 0.25	0.41 ± 0.24	0.69 ± 0.22	0.36 ± 0.30	1.04 ± 0.25
A_4	-0.16 ± 0.19	0.00 ± 0.27	0.03 ± 0.21	0.07 ± 0.19	-0.10 ± 0.18	-0.30 ± 0.25	-0.14 ± 0.21
A_5	0.00 ± 0.17	0.20 ± 0.23	0.08 ± 0.17	0.20 ± 0.15	0.07 ± 0.14	0.39 ± 0.21	0.39 ± 0.18
A_6							
χ^2	13.37	16.18	6.85	9.21	14.00	10.31	12.7
$\langle \chi^2 \rangle$	13	13	13	13	13	13	13
Confidence level (%)	42.0	23.9	91.0	75.7	37.4	66.9	47.2
$E_{c.m.}$ (MeV)	1628	1647	1660	1669	1674	1685	1695
Low-energy cutoff	1616	1632	1648	1656	1658	1670	1680
High-energy cutoff	1640	1662	1672	1682	1690	1700	1710
A_0	1.50 ± 0.11	1.72 ± 0.04	1.84 ± 0.04	2.10 ± 0.05	1.93 ± 0.04	2.09 ± 0.06	2.07 ± 0.07
A_1	1.43 ± 0.26	1.85 ± 0.09	1.85 ± 0.13	2.42 ± 0.11	2.13 ± 0.11	2.44 ± 0.16	2.69 ± 0.18
A_2	3.04 ± 0.36	3.65 ± 0.12	4.06 ± 0.17	4.94 ± 0.15	4.38 ± 0.15	5.07 ± 0.21	5.22 ± 0.24
A_3	2.21 ± 0.38	3.17 ± 0.12	3.57 ± 0.17	4.50 ± 0.15	4.04 ± 0.17	4.44 ± 0.23	4.77 ± 0.27
A_4	0.78 ± 0.30	1.16 ± 0.10	1.26 ± 0.14	1.83 ± 0.12	1.64 ± 0.17	2.00 ± 0.22	2.18 ± 0.25
A_5	1.11 ± 0.30	1.72 ± 0.10	1.82 ± 0.14	2.13 ± 0.12	1.98 ± 0.13	2.08 ± 0.15	2.16 ± 0.17
A_6					0.14 ± 0.13	-0.04 ± 0.15	0.17 ± 0.17
χ^2	9.75	11.89	4.86	20.09	14.75	14.91	9.23
$\langle \chi^2 \rangle$	13	14	14	14	13	13	13
Confidence level (%)	71.4	61.5	98.8	12.7	32.3	31.3	75.5
$E_{c.m.}$ (MeV)	1709	1720	1730	1740	1761	1762	1766
Low-energy cutoff	1696	1708	1716	1722	1750	1748	1754
High-energy cutoff	1720	1732	1744	1758	1772	1776	1778
A_0	1.88 ± 0.09	1.55 ± 0.11	1.43 ± 0.06	1.46 ± 0.04	1.09 ± 0.06	1.19 ± 0.04	1.25 ± 0.05
A_1	2.67 ± 0.24	2.35 ± 0.28	2.07 ± 0.16	2.30 ± 0.10	1.68 ± 0.17	1.89 ± 0.11	2.08 ± 0.13
A_2	4.75 ± 0.31	3.95 ± 0.38	3.40 ± 0.21	3.65 ± 0.13	2.61 ± 0.22	2.86 ± 0.15	3.15 ± 0.18
A_3	4.10 ± 0.34	3.45 ± 0.44	2.98 ± 0.23	3.01 ± 0.15	2.26 ± 0.25	2.38 ± 0.16	2.73 ± 0.20
A_4	2.01 ± 0.31	1.69 ± 0.42	1.37 ± 0.21	1.62 ± 0.14	1.08 ± 0.24	1.29 ± 0.16	1.61 ± 0.19
A_5	1.53 ± 0.22	1.20 ± 0.30	1.07 ± 0.16	1.06 ± 0.10	0.89 ± 0.18	0.72 ± 0.12	1.03 ± 0.14
A_6	-0.28 ± 0.21	0.32 ± 0.29	-0.37 ± 0.14	-0.14 ± 0.10	-0.14 ± 0.16	-0.17 ± 0.11	0.07 ± 0.13
χ^2	9.86	14.78	6.52	10.45	8.83	15.1	13.73
$\langle \chi^2 \rangle$	13	13	13	13	13	13	13
Confidence level (%)	70.5	32.2	92.5	65.7	78.5	30.2	39.3

TABLE V (Continued)

$E_{c.m.}$ (MeV)	1787	1806	1811	1821	1843	1853	1872
Low-energy cutoff	1774	1794	1796	1808	1828	1838	1856
High-energy cutoff	1800	1818	1826	1834	1858	1866	1888
A_0	0.99±0.05	1.06±0.09	1.10±0.05	1.02±0.04	1.04±0.04	0.99±0.04	1.00±0.03
A_1	1.62±0.13	1.82±0.22	1.82±0.13	1.71±0.12	1.80±0.10	1.67±0.10	1.73±0.08
A_2	2.33±0.17	2.76±0.31	2.64±0.18	2.38±0.16	2.52±0.13	2.34±0.13	2.37±0.11
A_3	1.94±0.19	2.35±0.35	2.30±0.19	2.14±0.18	2.28±0.14	2.17±0.14	2.31±0.12
A_4	0.79±0.18	1.28±0.34	1.26±0.18	1.12±0.17	1.31±0.13	1.32±0.14	1.45±0.11
A_5	0.41±0.14	0.64±0.26	0.53±0.14	0.50±0.13	0.61±0.10	0.52±0.11	0.56±0.09
A_6	-0.29±0.12	-0.03±0.25	-0.11±0.12	-0.10±0.11	-0.06±0.09	-0.03±0.10	0.11±0.08
χ^2	12.85	12.20	9.71	7.38	15.87	9.40	9.69
$\langle\chi^2\rangle$	13	13	13	13	13	13	13
Confidence level (%)	45.9	51.1	71.8	88.1	25.6	74.2	71.9
$E_{c.m.}$ (MeV)	1885	1904	1916	1933	1935	1963	1980
Low-energy cutoff	1872	1890	1902	1917	1920	1948	1966
High-energy cutoff	1898	1918	1930	1947	1950	1978	1994
A_0	0.98±0.04	0.95±0.03	0.87±0.03	0.93±0.04	0.83±0.04	0.81±0.02	0.78±0.03
A_1	1.74±0.11	1.74±0.08	1.59±0.08	1.79±0.10	1.53±0.10	1.56±0.06	1.56±0.07
A_2	2.39±0.15	2.36±0.11	2.05±0.11	2.40±0.14	2.02±0.14	2.09±0.09	2.01±0.10
A_3	2.37±0.16	2.40±0.11	2.13±0.11	2.55±0.15	2.13±0.15	2.20±0.09	2.15±0.10
A_4	1.60±0.14	1.67±0.10	1.37±0.10	1.79±0.13	1.47±0.13	1.65±0.09	1.59±0.09
A_5	0.64±0.11	0.76±0.08	0.52±0.08	0.87±0.10	0.68±0.11	0.84±0.07	0.80±0.07
A_6	0.21±0.09	0.25±0.07	0.20±0.06	0.41±0.09	0.34±0.09	0.45±0.05	0.37±0.05
χ^2	8.34	10.67	13.96	7.82	3.00	12.44	7.31
$\langle\chi^2\rangle$	13	13	13	13	13	13	13
Confidence level (%)	82.1	63.9	37.6	85.5	99.8	49.2	88.5

experiment. As usual in hydrogen-bubble-chamber experiments, the observed and theoretical χ^2 distributions agree satisfactorily provided that the theoretical χ^2 is scaled up by a factor. This "scale" factor is indicated in Fig. 8. Elastic events with $\chi^2 < 25$ were used in the subsequent analysis. To test the sensitivity to the χ^2 cutoff, the Legendre polynomial coefficients describing the angular distributions were computed for those events with $\chi^2 \leq 25$, and for the subsample of events with $\chi^2 \leq 10$. The values of the coefficients were unchanged within their errors.

The data were corrected for loss of events in which the scattering plane lies close to the camera axis. If the angle α is defined as the angle between the normal to the scattering plane and the camera axis, then a depletion of events is expected at 90° for forward-pion-production angles, where the protons have a small range. However, the data show this expected loss not only in the forward regions but also in the middle and backward regions. This latter loss of events is due to the previously mentioned bias of the POOH filter program

against steeply dipping tracks. Typical azimuthal distributions are shown in Fig. 9 for the forward, middle, and backward production regions. The bias is strongest in the forward regions. Corrections for these biases were made separately by regions of production angle and energy and are listed in Table IV.

IV. RESULTS

In this section we present the results of our measurement of the π^-p elastic-scattering cross sections. In determining the angular distributions the c.m. energy cutoffs of Table V were used. Our data were normalized to counter-experiment results in the range of scattering angles, $-0.8 \leq \cos\theta < 0.7$, where the experimental biases are not a serious problem for either counters or HBC. Specifically, we have used the data of Duke *et al.*,²⁰ Helland *et al.*,²¹ and Ogden *et al.*²² It should be noted that this normalization region contributes only (20–30)% of the total elastic cross section, and that it varies slowly as a function of energy throughout the region investigated (see Fig. 10).

Thus, our measurement of the total cross section, and of the sharply varying energy dependencies, is only weakly dependent on the fact that we have normalized to the counter work.

The elastic-scattering angular distributions are presented in Fig. 11. The data are available in tabular form elsewhere.²³ The distributions extend up to $\cos\theta = 0.90$ below 1647 MeV, and up to $\cos\theta = 0.95$ at higher energies. At more-forward angles the recoiling proton has nearly zero range.

The smooth curves superposed on the data in Fig. 11 represent the best fit to a series expansion in Legendre polynomials, where

$$\frac{d\sigma}{d\Omega} = \sum_n A_n P_n(\cos\theta).$$

A fit to order $n=5$ was sufficient below 1674 MeV, and to order $n=6$ at higher energies. Table V lists the Legendre coefficients A_n for each energy, along with the χ^2 and confidence level describing the fit to the data. These coefficients are plotted in Fig. 12 along with those of other experiments.^{20, 22} The agreement is good.

The total elastic cross section was determined from the Legendre fit to the data using the relation

$$\sigma_{el} = 4\pi A_0.$$

The elastic cross section is shown in Fig. 10 compared to the cross sections of the counter experiments.²⁰⁻²²

The forward cross section may be extrapolated from the Legendre coefficients according to

$$\frac{d\sigma}{d\Omega}(\theta=0) = \sum_n A_n.$$

The forward elastic cross sections thus determined are the data points in Fig. 13. The smooth curve represents the forward cross section predicted by Carter.²⁴ The real part of the forward scattering amplitude was calculated from partial-wave dispersion relations, while the imaginary part was obtained from the optical theorem using the recent precision total-cross-section measurements of Carter *et al.*²⁵ The curve shows a marked shift toward the low-energy side of the third resonance peak. This shift reflects the shift of the data of Carter *et al.* compared to other experiments,²⁶⁻²⁹ as seen in Fig. 14.

The behavior of the Legendre coefficients reflects qualitatively the resonance structure. The fact that all coefficients up to and including A_5 show a strong peak near 1690 MeV indicates the presence of D_5 and F_5 resonances. Furthermore, the absence of any rapid variation or change of sign of A_5 implies that the D_5 and F_5 have a constant phase difference near the resonance peak.

The presence of a D_3 resonance is signaled by the bump in A_2 near 1520 MeV. The similar bump in A_1 can be attributed to interference of the D_3 with a P_1 resonance. The sign change in A_3 reflects interference of the D_3 with the P_3 resonance. (They are more than 90° out of phase here.) Finally, the fact that A_4 is consistent with zero implies zero interference between D_3 and D_5 (i. e., these waves must be about 90° out of phase).

V. DISCUSSION

While the Legendre coefficients indicate qualitatively the behavior of the dominant partial waves, more-precise quantitative information is obtained from phase-shift analyses. The dynamics of the interaction of a pion with a nucleon are contained in the partial-wave amplitudes T_l^\pm , $J = l \pm \frac{1}{2}$. It is the behavior of these amplitudes which a phase-shift analysis seeks to discover. The first step is thus to select some parametrization for these amplitudes. The T -matrix elements are related to the center-of-mass scattering amplitude through the following relations³⁰:

$$M = f(\theta) + g(\theta)\vec{\sigma} \cdot \hat{n},$$

where

$$\hat{n} = \vec{k}_i \times \vec{k}_f / |\vec{k}_i \times \vec{k}_f|,$$

$$f(\theta) = \frac{1}{k} \sum_l [(l+1)T_l^+ + lT_l^-] P_l^1(\cos\theta),$$

and

$$g(\theta) = \frac{i}{k} \sum_l (T_l^+ - T_l^-) P_l^1(\cos\theta).$$

$f(\theta)$ and $g(\theta)$ are the spin-nonflip and spin-flip scattering amplitudes.

The differential cross section and polarization are then given by

$$\frac{d\sigma}{d\Omega} = |M|^2 = |f|^2 + |g|^2,$$

$$I\vec{P} = 2\text{Re}(f^*g)\hat{n}.$$

The cross sections and polarizations predicted by the given parameters are compared with the experimental data and the parameters adjusted until a good fit is obtained. At the same time the parameters may be constrained by theoretical input. For example, all phase-shift analyses require the parameters to satisfy some form of unitarity.

There are two main types of phase-shift analysis: energy-independent and energy-dependent. Examples of the former type are the Saclay,¹ Berkeley,⁶ and CERN⁷ analyses, while the analyses of Roper,⁴ Chilton,² and Glasgow³¹ are examples of the latter type. The different methods are reviewed and compared elsewhere.³²

In Figs. 15-18 our elastic cross section and the differential cross section at six typical energies

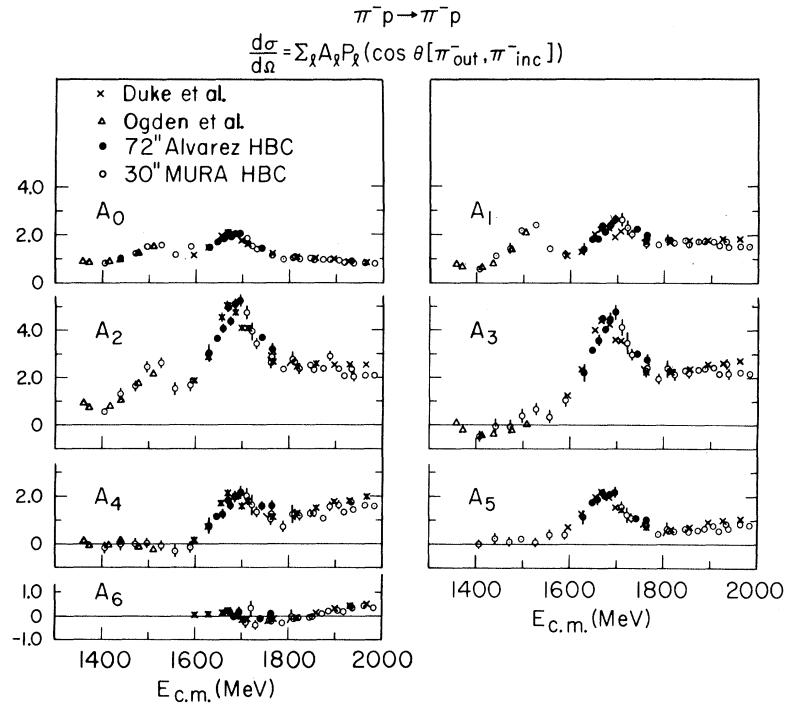


FIG. 12. Legendre coefficients from fit to π^-p differential cross sections.

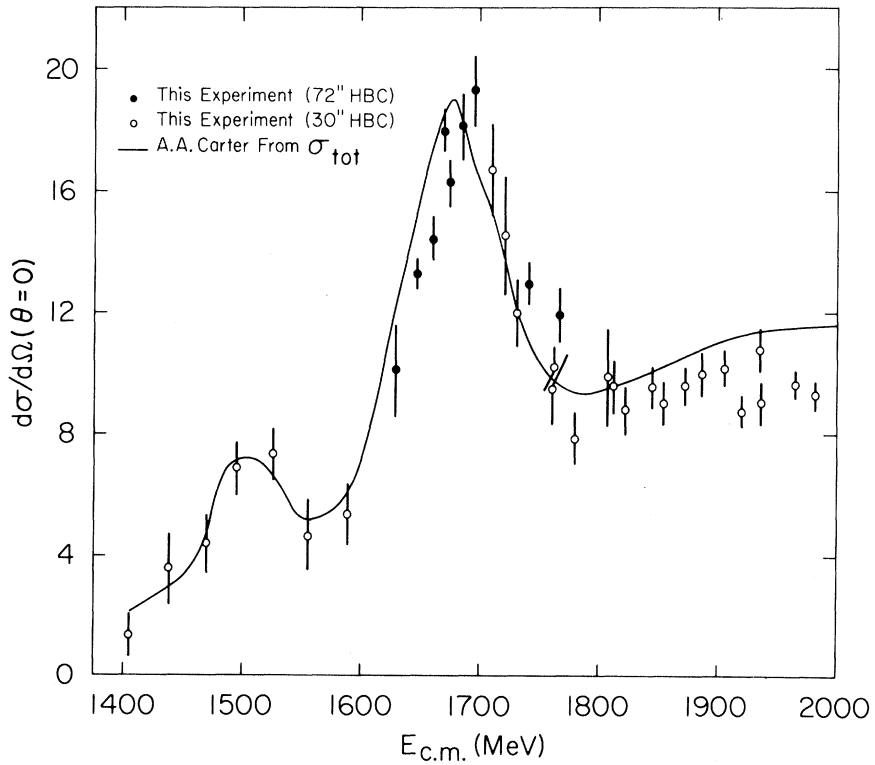


FIG. 13. Forward π^-p elastic cross section measured in this experiment. The smooth curve is calculated by Carter (Ref. 24) using dispersion relations and the total π^-p cross-section measurements of Carter *et al.* (Ref. 25).

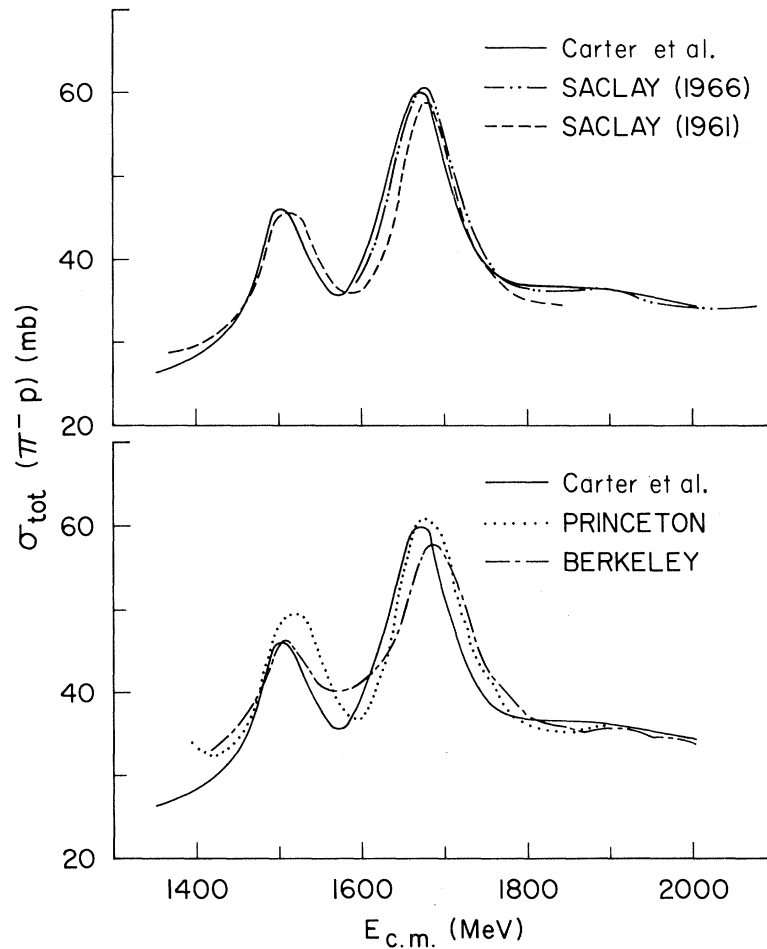


FIG. 14. Total $\pi^- p$ cross sections measured by Carter *et al.* (Ref. 25), Berkeley (Ref. 26), Princeton (Ref. 27), Saclay (1961) (Ref. 28), and Saclay (1966) (Ref. 29).

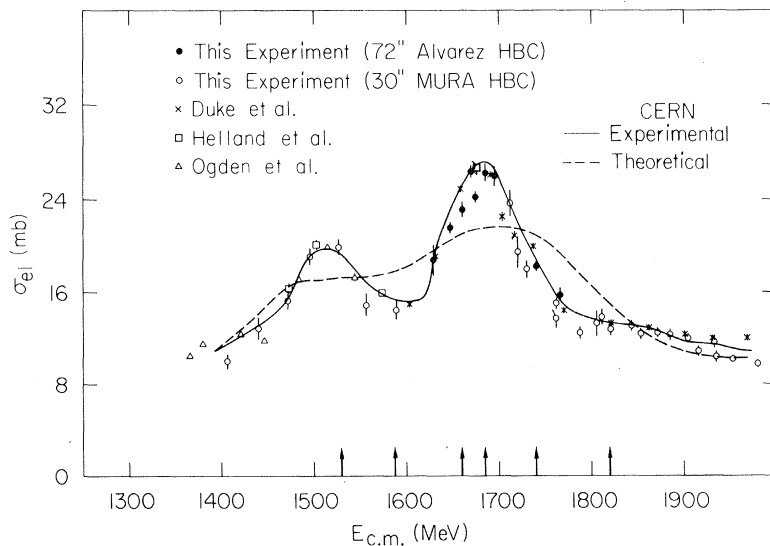


FIG. 15. $\pi^- p$ elastic-cross-section measurements of Duke *et al.* (Ref. 20), Helland *et al.* (Ref. 21), Ogden *et al.* (Ref. 22), and this experiment. Solid and dashed lines represent the $\pi^- p$ elastic cross section predicted by CERN-Experimental and CERN-Theoretical phase shifts, respectively. The arrows indicate the energies chosen for differential-cross-section comparison.

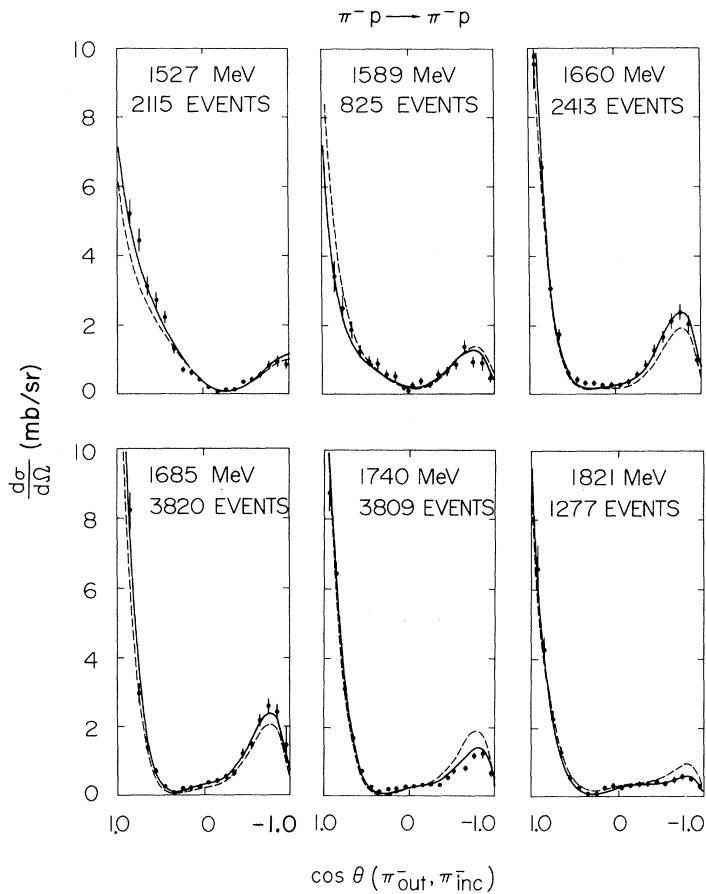


FIG. 16. π^-p differential cross section at six energies measured in this experiment. Solid and dashed lines are the predictions of CERN-Experimental and CERN-Theoretical phase shifts.

(shown by arrows in Figs. 15 and 17) are compared to the predictions of the various phase-shift analyses. In Fig. 15 the CERN solutions are shown. The comparison of "CERN-Theoretical" with the data has already been dealt with extensively in the

literature,³³ while "CERN-Experimental" is seen to represent the data well, both in the cross section and in the differential cross section (Fig. 16). In Figs. 17-18 the predictions of the Saclay, Berkeley, and Glasgow work are shown to repre-

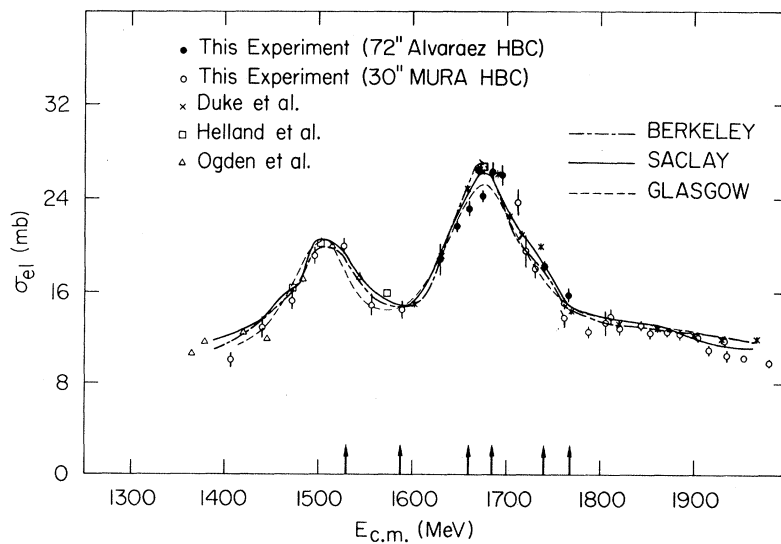


FIG. 17. π^-p elastic cross section predicted by Saclay (Ref. 1), Berkeley (Ref. 6), and Glasgow (Ref. 31) compared to the same data as in Fig. 15.

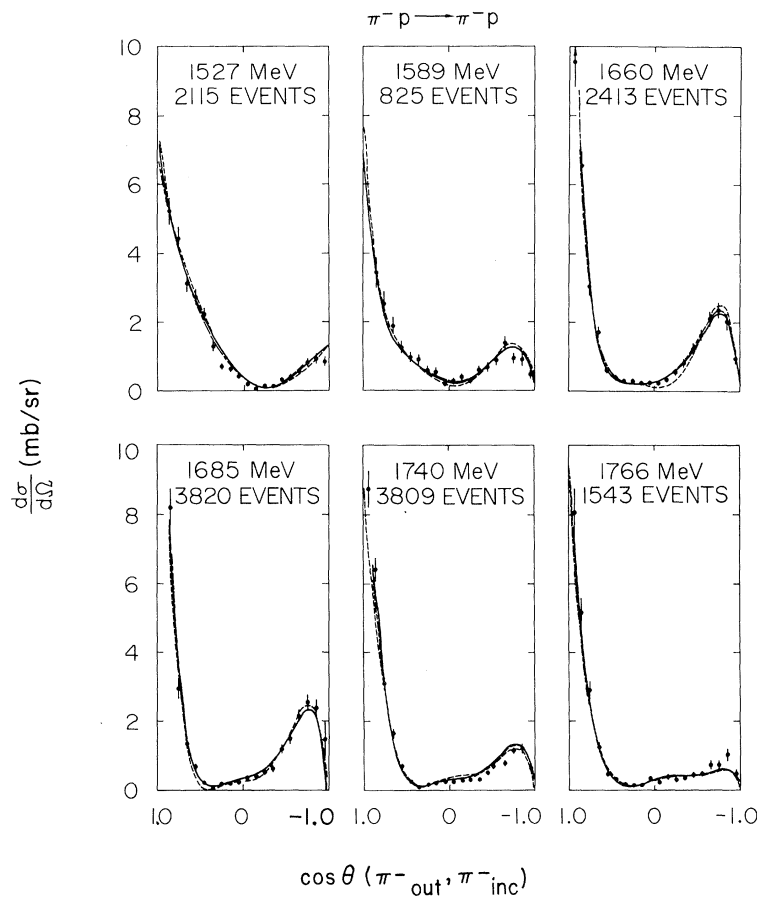


FIG. 18. π^-p differential cross section predicted by Saclay (Ref. 1), Berkeley (Ref. 6), and Glasgow (Ref. 31) compared to the experimental data.

sent the data fairly well.

VI. CONCLUSION

The new elastic-scattering data presented here confirm the general behavior shown by previous experiments. Because this experiment spans a wide energy region in a systematic way, it offers useful information for phenomenological analysis of πN scattering.

ACKNOWLEDGMENTS

We wish to thank F. S. Crawford, Jr. and J. A.

Anderson for leading the LRL HBC film and helping to make that part of the experiment possible. We also wish to thank the LRL Spiral Reader crew and especially G. R. Lynch and L. J. Lloyd for their help and assistance in measuring the film, and the SLAC CDA staff for their scanning effort. Finally, we wish to acknowledge the valuable assistance at the early stage of the experiment of A. Minten and R. Diebold.

*Work supported by the U. S. Atomic Energy Commission.

†Present address is CERN, Geneva, Switzerland.

‡Present address is University of California, Riverside, Calif.

§Present address is Department of Nuclear Physics, Oxford University, Oxford, England.

|| Present address is University of California, Irvine, Calif.

**Present address is DESY, Hamburg, West Germany.

¹P. Bareyre, C. Bricman, A. V. Stirling, and G. Villet, Phys. Letters 18, 342 (1965); P. Bareyre, C. Bricman,

and G. Villet, Phys. Rev. 165, 1730 (1968).

²B. H. Bransden, P. J. O'Donnell, and R. G. Moorhouse, Phys. Letters 11, 339 (1964); Phys. Rev. 139, B1566 (1965); Proc. Roy. Soc. (London) A289, 538 (1966); Phys. Letters 19, 420 (1965).

³P. Auvil, A. Donnachie, A. T. Lea, and C. Lovelace, Phys. Letters 12, 76 (1964); 19, 148 (1965).

⁴L. D. Roper, Phys. Rev. Letters 12, 340 (1964); L. D. Roper, R. M. Wright, and B. T. Feld, Phys. Rev. 138, B190 (1965); L. D. Roper and R. M. Wright, *ibid.* 138, B921 (1965).

⁵R. J. Cence, Phys. Letters 20, 306 (1966).

⁶C. H. Johnson, Lawrence Radiation Laboratory Report No. UCRL-17683, 1967 (unpublished).

⁷A. Donnachie, R. G. Kirsopp, and C. Lovelace, Phys. Letters 26B, 161 (1968); C. Lovelace, in *Proceedings of the International Conference on Elementary Particles, Heidelberg, Germany, 1967*, edited by H. Filthuth (North-Holland, Amsterdam, 1967), p. 79; C. Lovelace, in *Proceedings of the Conference on πN Scattering, Irvine California, 1967*, edited by G. L. Shaw and D. Y. Wong (Wiley, New York, 1967); CERN Report No. CERN-TH-839, 1967 (unpublished).

⁸R. G. Moorhouse, Ann. Rev. Nucl. Sci. 19, 301 (1969).

⁹D. Herndon, A. Barbaro-Galtieri, and A. H. Rosenfeld, Lawrence Radiation Laboratory Report No. UCRL-20030 πN , 1970 (unpublished).

¹⁰G. Giacomelli, P. Pini, and S. Stagni, CERN Report No. CERN/HERA 69-1 (unpublished).

¹¹G. L. Shaw and D. Y. Wong, in *Proceedings of the Conference on πN Scattering, Irvine, California, 1967*, Ref. 7.

¹²The contents of this table are taken from Particle Data Group, Phys. Letters 33B, 1 (1967). The various phase-shift analyses are identified as (1) P. Bareyre, C. Bricman, and G. Villet, Phys. Rev. 165, 1730 (1968); (2) P. Bareyre, C. Bricman, and G. Villet, Phys. Rev. 165, 1730 (1968); (3) Claiborne H. Johnson, Jr., Lawrence Radiation Laboratory Report No. UCRL-17683, 1967 (unpublished); (4) A. Donnachie, R. G. Kirsopp, and C. Lovelace, Phys. Rev. Letters 26B, 161 (1968); (5) A. Donnachie, R. G. Kirsopp, and C. Lovelace, Phys. Rev. Letters 26B, 161 (1968); (6) R. G. Kirsopp, Ph. D. thesis (unpublished); (7) A. T. Davies, Nucl. Phys. B21, 359 (1970); (8) A. T. Davies, Nucl. Phys. B21, 359 (1970); (9) A. T. Lea, G. C. Oades, D. L. Ward, I. M. Cowan, W. M. Gibson, R. S. Gilmore, J. Malos, V. J. Smith, and M. A. R. Kemp, Rutherford Laboratory Report No. RPP/H/57 (unpublished). For a thorough discussion of each solution, we refer the reader to the original papers and the review articles.

¹³F. S. Crawford, in *Proceedings of the International Conference on High Energy Physics, CERN, 1962*, edited by J. Prentki (CERN, Geneva, Switzerland, 1962), p. 270; J. A. Anderson, Lawrence Radiation Laboratory Report No. UCRL 10838, 1963 (unpublished); J. Anderson, F. S. Crawford, Jr., and J. C. Doyle, Phys. Rev. 152, 1139 (1967); J. C. Doyle, F. S. Crawford, Jr., and J. A. Anderson, Phys. Rev. 165, 1483 (1968); J. C. Doyle, Lawrence Radiation Laboratory Report No. UCRL-18139, 1969 (unpublished).

¹⁴T. H. Fields, E. L. Goldwasser, and U. E. Kruse, Argonne National Laboratory Internal Report No. THF/ELG/UEK-1, 1961 (unpublished).

¹⁵S. Wolf, N. Schmitz, L. Lloyd, W. Laskar, F. Crawford, Jr., J. Button, J. Anderson, and G. Alexander, Rev. Mod. Phys. 33, 439 (1961).

¹⁶SLAC physics note, APE Data Processing Note No. 1 (unpublished).

¹⁷J. Lynch, Lawrence Radiation Laboratory Report No. UCRL-17238, 1967 (unpublished).

¹⁸J. Burkhard, in *Proceedings of a Conference on Flying Spot Devices at Columbia, 1965* (unpublished).

¹⁹Basically this shift is due to the fact that E and p are correlated through the measured parameters. The correlation is such that $m^2 = E^2 - p^2$ is shifted to more-negative values. This shift can be about as large as δm^2 , especially for $m^2 = 0$. See S. Wojcicki and F. Solmitz, Alvarez Group Memo No. 367 (unpublished).

²⁰P. J. Duke, D. P. Jones, M. A. R. Kemp, P. G. Murphy, J. D. Prentice, and J. J. Thresher, Phys. Rev. 149, 1077 (1966).

²¹J. A. Helland, T. J. Devlin, D. E. Hagge, M. J. Longo, B. J. Moyer, and C. D. Wood, Phys. Rev. 134, B1062 (1964); J. A. Helland, C. D. Wood, T. J. Devlin, D. E. Hagge, M. J. Longo, B. J. Moyer, and V. Perez-Mendez, Phys. Rev. 134, B1079 (1964).

²²D. M. Ogden, D. E. Hagge, J. A. Helland, M. Banner, J. F. Detoeuf, and J. Leiger, Phys. Rev. 137, B115 (1965).

²³A. D. Brody, R. J. Cashmore, A. Kernan, D. W. G. S. Leith, B. S. Levi, B. C. Shen, J. P. Berge, D. J. Herndon, R. Longacre, L. R. Price, A. H. Rosenfeld, and P. Söding, SLAC Report No. SLAC-PUB-789, Supplement 1 (unpublished).

²⁴A. A. Carter, Cavendish Laboratory Internal Report (unpublished).

²⁵A. A. Carter, F. K. Riley, R. J. Tapper, D. V. Bugg, R. S. Gilmore, K. M. Knight, D. C. Salter, G. H. Stafford, E. J. N. Wilson, J. D. Davies, J. D. Dowell, P. M. Hattersley, R. J. Homer, and A. W. O'Dell, Phys. Rev. 168, 1457 (1968).

²⁶T. J. Devlin, B. J. Moyer, and V. Perez-Mendez, Phys. Rev. 125, 690 (1962).

²⁷T. J. Devlin, J. Solomon, and G. Bertsch, Phys. Rev. Letters 14, 1031 (1965).

²⁸J. C. Brisson, J. F. Detoeuf, P. Falk-Variant, L. Van Rensburg, G. Valladas, and L. C. L. Yan, Nuovo Cimento 19, 210 (1961).

²⁹G. Bizard, J. Duchon, J. Sequinot, J. Yonnet, P. Bareyre, C. Bricman, G. Valladas, and G. Villet, Nuovo Cimento 44, 999 (1966); M. Banner, P. Bareyre, and C. Bricman, Nuovo Cimento (to be published); A. Stirling *et al.*, cited by B. Ambland *et al.*, Phys. Letters 10, 140 (1964).

³⁰M. L. Goldberger and K. M. Watson, *Collision Theory* (Wiley, New York 1964).

³¹A. T. Davies, Nucl. Phys. B21, 359 (1970).

³²A. D. Brody, R. J. Cashmore, A. Kernan, D. W. G. S. Leith, B. S. Levi, B. C. Shen, J. P. Berge, D. J. Herndon, R. Longacre, L. R. Price, A. H. Rosenfeld, and P. Söding, SLAC Report No. SLAC-PUB-789, Supplement 2 (unpublished).

³³A. D. Brody, D. W. G. S. Leith, B. G. Levi, B. C. Shen, D. Herndon, R. Longacre, L. Price, A. H. Rosenfeld, and P. Söding, Phys. Rev. Letters 22, 1401 (1969); A. Donnachie and C. Lovelace, Phys. Rev. D 1, 956 (1970) (reply); A. D. Brody *et al.*, SLAC Report No. SLAC-PUB-709 (reply) (unpublished).